ChemComm

Accepted Manuscript

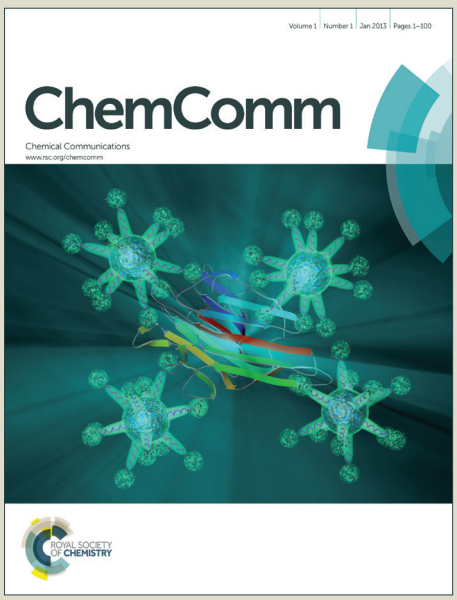

ROYAL SOCIETY OF CHEMISTRY

www.rsc.org/chemcomm

Journal Name

RSCPublishing

COMMUNICATION

High catalytic activity for water oxidation based on nanostructured nickel phosphide precursors

Ali Han, Huanlin Chen, Zijun Sun, Jun Xu, Pingwu Du*

Cite this: DOI: 10.1039/x0xx00000x

Received 00th January 2012,
Accepted 00th January 2012

DOI: 10.1039/x0xx00000x

www.rsc.org/

For the first time, noble-metal-free nickel phosphide (Ni_2P) was used as an excellent catalyst precursor for water oxidation catalysis. The lowest onset potential was observed at ~1.54 V (vs. RHE) and a Tafel slope of 60 mV/dec was obtained in alkaline solution (pH =13.6).

Hydrogen production through photo- and electro-catalytic water splitting has attracted much attention in the last few decades.[1-2] The water splitting reaction contains two half-reactions: hydrogen evolution reaction (HER) and water oxidation reaction. Catalysts play very important roles in highly promoting both HER and water oxidation. In nature, the $CaMn_4O_5$ active site in the oxygen evolution center of photosystem II serves as the catalyst for water oxidation, in that it can assist the O-H bond breaking and the formation of O-O to evolve O_2.[3-4] Inspired by nature, a variety of materials and molecular metal complexes made of earth-abundant elements have been widely studied as catalysts for the water oxidation reaction, such as the materials based on the elements Mn,[5-6] Co,[7-9] Ni,[10-11] Fe,[12-13] and Cu elements.[14-16]. Despite these studies, for the purpose of future application, there is still a demand for highly efficient, robust, and low-cost water oxidation catalysts.

Nickel phosphide, a material made of earth-abundant nickel element, has been recently reported as an efficient HER catalyst with low overpotentials under different pH values.[17-19] Nickel phosphide was not expected to have good prospects for catalytic water oxidation because it was usually used for reduction reaction. And to the best of our knowledge, the use of nickel phosphide for catalytic water oxidation has not received prior investigation. There are a few metal oxide and metal sulfide materials, such as CoO_x,[20] NiO_x,[11] and NiS_x,[21-22] have been reported as bifunctional catalysts for catalyzing both HER and water oxidation reaction. Inspired by these studies, herein we report on the use of Ni_2P nanowires and nanoparticles as highly active catalysts precursors for water oxidation. Our results indicated that the nanowire-based catalyst showed a low onset potential at ~1.54 V (vs. RHE) at pH 13.6 and a Faradic efficiency of > 92% was achieved under an overpotential of 360 mV. All of our results demonstrate that Ni_2P nanowires have high activity for water oxidation in alkaline solution.

Nanostructured nickel phosphide (Ni_2P) materials with two different morphologies (nanowires and nanoparticles) were successfully synthesized and the experimental details can be found in supplementary information. The morphologies of the as-prepared Ni_2P nanowires and Ni_2P nanoparticles were investigated by transmission electron microscopy (TEM). Figure 1a shows the TEM images of Ni_2P materials, demonstrating the nanowire morphology with a diameter of 4~7 nm and a length of 100-300 nm. A high-resolution TEM image of the nanowire material is shown in the inset of Figure 1b. The average length is ~5 nm, which is consistent with the result from the TEM image. In addition, the HR-TEM image gave a crystal lattice spacing of ~0.34 nm, corresponding to the (001) plane of Ni_2P (PDF#74-1385) (Figure 1b, inset). The TEM image of the Ni_2P nanoparticles is shown in Figure S1a. The nanoparticles are aggregated with each other and the size of nanoparticles is in a range of 20-50 nm. The high-resolution TEM (HR-TEM) image in Figure S1b also shows a lattice spacing of 0.34 nm of Ni_2P (001).

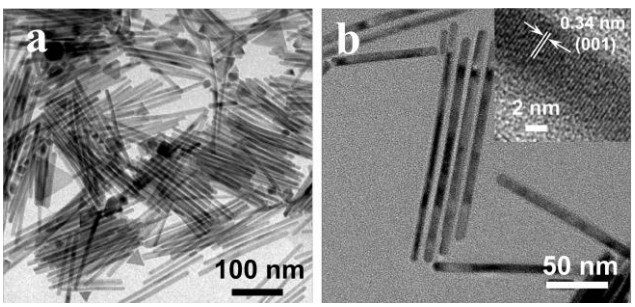

Figure 1. (a) and (b) TEM images of Ni_2P nanowires. The inset image is the HRTEM image of Ni_2P nanowires.

Powder X-ray diffraction (XRD) patterns of the as-synthesized Ni_2P nanowires and Ni_2P nanoparticles are shown in Figure 2a. The appreciable diffraction peaks at $2\theta = 40.77$, 44.59, 47.45, 54.16, 66.54, 72.64, and 74.34 are assigned to the (111), (201), (210), (300), (310),

(311), and (400) planes of hexagonal Ni_2P (PDF#74-1385), respectively. It should be noted that the diffraction peaks of Ni_2P nanowires (black plot) are much broader than Ni_2P nanoparticles (red plot). In addition, the intensity of the (300) peak in Ni_2P nanowires is relatively higher. These observations probably result from the anisotropic nanostructure, in particular the increased dimension in the long axis of Ni_2P nanowires. The peak of (300) is also a feature of the increased dimension in the long axis of the nanocrystals. Such a distinctive peak has also existed in other nanowire samples.[23-24]

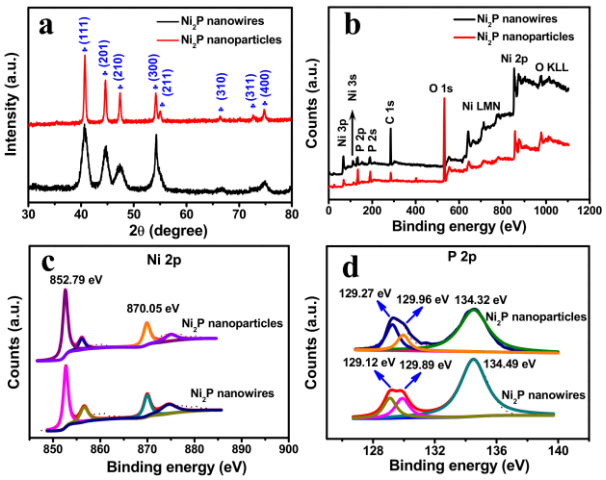

Figure 2. (a) X-ray diffraction patterns of the as-prepared Ni_2P nanowires (black) and Ni_2P nanoparticles (red); (b) XPS survey data of Ni_2P nanowires (black) and Ni_2P nanoparticles (red); (c) high resolution XPS spectra of Ni 2p; (d) high resolution XPS spectra of P 2p.

The XPS spectra of Ni_2P samples were measured to identify the surface chemical composition and valence states. The XPS survey scans in Figure 2b show the presence of Ni, P, O, and C elements. The binding energies were corrected according to the C element at 285.0 eV. The high resolution XPS spectra of Ni and P elements from Ni_2P nanowires are shown in Figures 2c and 2d. The peaks at 852.79 eV and 870.05 eV are assigned to Ni $2p_{3/2}$ and Ni $2p_{1/2}$ binding energies, respectively.[18, 25] The high resolution spectrum of P 2p shows two peaks located at 129.12 eV and 129.89 eV, corresponding to P $2p_{3/2}$ and P $2p_{1/2}$, respectively. The other peak at 133.49 eV was probably from partial oxidation of Ni_2P on the surface.[23, 26-27] As for the Ni_2P nanoparticles, the peaks for Ni 2p have features similar to those of the Ni_2P nanowires although the spectrum of P 2p at 134.32 eV showed a slight shift compared to P 2p of Ni_2P nanowires at 133.49 eV.

The energy-dispersive X-ray spectroscopy (EDX) spectra of Ni_2P nanowires and Ni_2P nanoparticles confirm the presence of Ni and P elements, as shown in Figures S2a and S2b. Both samples also contain Pt and O elements. Pt was sprayed on the samples to increase the conductivity for EDX measurement. The O was probably from the absorbed gas molecules, a phenomenon which also is seen for other metal phosphides.[18, 24] More importantly, both Ni_2P samples exhibit Ni and P elements with an atom ratio at ~2:1, which is consistent with the stoichiometric ratio of elements in Ni_2P materials.

The electrocatalytic activity of the Ni_2P material for water oxidation was investigated in alkaline solution (1.0 M KOH, pH ~13.6) using a standard three-electrode system. The details of the electrochemical methods can be found in the supplementary information. Ni_2P nanowires were loaded on FTO glass plate (0.1 mg/cm^2 with nafion) as the working electrode. Figure 3a shows cyclic voltammetry (CV) scans of Ni_2P nanowires with different cycles at a scan rate of 50 mV/s. The quasi-reversible oxidation peak at 1.38 V (vs. RHE, note: all the potentials in this paper are versus RHE) is tentatively assigned to the oxidation of Ni_2P. An obvious oxidation wave appeared in the first scan with an onset potential of ~1.60 V, accompanied by a large amount of gas bubbles on the surface of the working electrode. The gas bubbles were confirmed to be oxygen by both gas chromatography and a fluorescence-based oxygen sensor. Therefore, this oxidation wave is attributed to a water oxidation process. With continuous CV scans, the onset potential for water oxidation was decreased and the catalytic current density was enhanced under the same applied potential, indicating that the electroactive species formed on the electrode surface during CV scans. A stable current density was achieved after 200 cycles and no deactivation was observed from the first cycle to the 500th cycle. The lowest onset potential of ~1.54 V was achieved for Ni_2P nanowires, a figure which is comparable to many metal oxide-based water oxidation catalysts such as Co_3O_4/N-graphene (1.63 V vs. RHE, pH 14),[28] N/C–NiO_x (1.7 V vs. RHE, pH 13),[29] $NiCo_2O_4$ (1.52 V vs. RHE, pH 13.6),[30] and $Zn_xCo_{3-x}O_4$ (1.55 V vs. RHE, pH 14).[31] Therefore, the present Ni_2P nanowire material is among the most efficient reported noble-metal-free electrocatalysts for water oxidation in alkaline solutions.

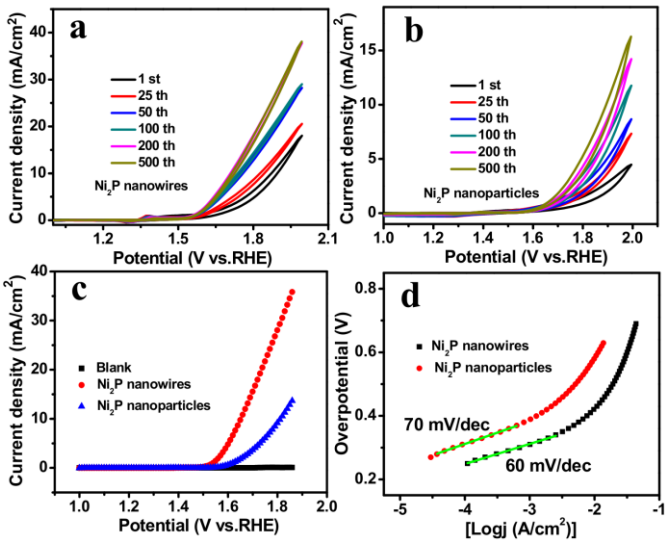

Figure 3. (a) CV scans using FTO electrode loading 0.1 mg/cm^2 Ni_2P nanowires as the working electrode in 1.0 M KOH (pH = 13.6). The scan rate was 50 mV s^{-1} and iR drop was applied; (b) CV scans using FTO electrode loading 0.1 mg/cm^2 Ni_2P nanoparticles as the working electrode in 1.0 M KOH (pH = 13.6). The scan rate was 50 mV s^{-1} and iR drop was applied; (c) Polarization curves for Ni_2P nanowires, and nanoparticles on FTO after CV scans for 500 cycles in 1.0 M KOH. Bare FTO electrode was used for comparison. (d) The Tafel plots of Ni_2P nanowires and nanoparticles obtained from the polarization curves in Figure 3c.

For comparison, Ni_2P nanoparticles on FTO were used for CV scans, as shown in Figure 3b. During the scans, appreciable catalytic waves for water oxidation appeared but the catalytic current densities were much lower than that for nanowires. In the beginning, the oxidation wave presented a quite high onset potential of 1.67 V for water oxidation. After 500 cycles, the onset potential was negatively shifted to only ~1.63 V but the current density was significantly enhanced. The final onset potential was about 100 mV higher than that for Ni_2P nanowires. These results indicate that the Ni_2P nanowires are much more active than nanoparticles under the same conditions.

To further study the catalytic properties, the above two working electrodes prepared after 500 CV scans were used for linear sweep voltammetry (LSV) at a scan rate of 5 mV/s (Figure 3c). Under such a scan rate, the onset potentials for water oxidation are clearly observed. The results show an onset potential at ~1.54 V for Ni_2P nanowires and ~1.61 V for Ni_2P nanoparticles, which is nearly the

same as the observations by CV scans. Note that bare FTO electrode without loading Ni_2P materials shows negligible catalytic current under an applied potential less than 1.88 V, indicating the important role of Ni_2P for catalytic water oxidation. From the LSV data in Figure 3c, we can see that a current density of 10 mA/cm^2 can be achieved with an overpotential of only ~400 mV for Ni_2P nanowires and ~500 mV for Ni_2P nanoparticles. For comparison, a simple nickel salt ($NiCl_2$) was used as a precursor for water oxidation. However, $NiCl_2$ was not soluble in strong basic solution. Then, we initially used $NiCl_2$ (~1.34 μmol) as the precursor in 0.1 M KPi (pH = 7.0) to obtain NiO_x-based catalyst film. After 2 h of electrolysis under a potential of 1.3 V (vs. Ag/AgCl), the film was cleaned by water and transferred into 1.0 M KOH for electrocatalysis. LSV results in Figure S3 showed the catalyst derived from Ni_2P nanowires had much higher catalytic activity than that obtained from $NiCl_2$.

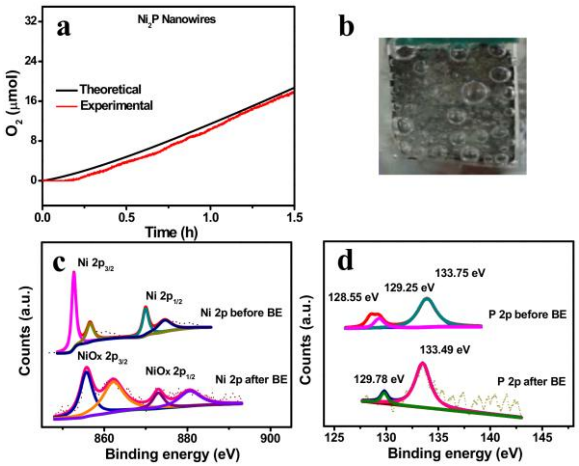

Figure 4. (a) The Faradic efficiency of Ni_2P nanowires on FTO in 1.0 M KOH under an overpotential of 360 mV. (b) Oxygen gas bubbles during electrolysis using Ni_2P nanowires. (c) High resolution XPS spectra of Ni 2p before (top) and after electrolysis (bottom) for 10 h; (d) High resolution XPS spectra of P 2p before (top) and after electrolysis (bottom) for 10 h.

The reaction kinetics of Ni_2P nanomaterials can be studied by the Tafel plot. The current density (j) under various potentials was obtained from the LSV data. The Tafel plots were then calculated by a function of the overpotential (η) vs. the Nernstian potential for water oxidation (Figure 3d). The slope of the Tafel plot for Ni_2P nanowires is ~60 mV/dec, indicating a very efficient kinetics for the water oxidation process. From the plot, an appreciable current density at η ~250 mV is observed. A current density of ~1.0 mA/cm^2 required η = 310 mV. In contrast, the Ni_2P nanoparticles show a higher Tafel slope of ~70 mV/dec, indicating that Ni_2P nanoparticles material is less active than Ni_2P nanowire material. The high activity of Ni_2P nanowires for water oxidation activity can probably be attributed to its one dimensional (1D) structural feature providing more active sites than nanoparticles. The Faraday efficiencies for O_2 evolution of Ni_2P-based catalysts on FTO (0.5 cm^2 surface area, 0.1 mg/cm^2 loading) were estimated under an overpotential of 360 mV for 1.5 h. The electrolysis experiments resulted in evolution of 18.7 μmol O_2 for Ni_2P nanowires. The amounts of evolved O_2 showed a Faradic efficiency of > 92% (Figure 4a). A large amount of gas bubbles on the surface of the working electrode were produced during electrolysis for the Faradic efficiency measurement (Figure 4b).

To further investigate the composition and valence states of the Ni_2P-based catalysts, XPS spectra were examined after bulk electrolysis for 10 h (Figures 4c and 4d). Significant differences can be seen from the high resolution spectra of Ni 2p and P 2p. The binding energies of Ni 2p at 855.7 eV ($2p_{3/2}$) and 873.0 eV ($2p_{1/2}$) indicate the formation of NiO_x (~855.6 eV).[11] As for P 2p, an obvious oxidation peak at 133.6 eV appears, suggesting that P in Ni_2P is probably oxidized to produce phosphate species (~133.6 eV),[23, 26-27] which might help proton transfer during water oxidation catalysis.[7] Therefore, Ni_2P materials served as active catalyst precursors to catalyze water oxidation at low overpotentials. SEM images of Ni_2P after electrolysis were also measured (Figure S4). The NiO_x obtained from Ni_2P nanoparticles showed aggregated nanoparticles (Figure S4a) and the morphology of the NiO_x from Ni_2P nanowires still showed many nanowires and short nanowires have been observed (Figure S4b).

Conclusions

In summary, this is the first report that nanostructured Ni_2P materials have been studied for water oxidation catalysis. The results show that Ni_2P nanowires material is more active than Ni_2P nanoparticle material and the lowest onset potential of ~1.54 V can be achieved using Ni_2P nanowires. The Faradic efficiency was more than 92% under an overpotential of 360 mV. The electrochemical measurements demonstrated that Ni_2P nanowire material is an excellent electrocatalyst for water oxidation under alkaline conditions. Further XPS analysis indicated that Ni_2P is probably a catalyst precursor during water oxidation catalysis.

This work was financially supported by NSFC (21271166, 21473170), the Fundamental Research Funds for the Central Universities, the Program for New Century Excellent Talents in University (NCET), and the Thousand Young Talents Program.

Notes and references

[a]*Key Laboratory of Materials for Energy Conversion, Chinese Academy of Sciences, Department of Materials Science and Engineering, iChEM(Collaborative Innovation Center of Chemistry for Energy Materials), University of Science and Technology of China, 96 Jinzhai Road, Hefei, Anhui Province, 230026, P. R. China. Fax: 86-551-63606207; E-mail: dupingwu@ustc.edu.cn*

† Electronic Supplementary Information (ESI) available: Experimental details, figures and so on. See DOI: 10.1039/c000000x/

1 N. S. Lewis, D. G. Nocera, *Proc. Natl. Acad. Sci. U.S.A.* 2006, ***103***, 15729-15735.
2 H. B. Gray, *Nat. Chem.* 2009, ***1***, 7-7.
3 M. Suga, F. Akita, K. Hirata, G. Ueno, H. Murakami, Y. Nakajima, T. Shimizu, K. Yamashita, M. Yamamoto, H. Ago, J. R. Shen, *Nature* 2015, ***517***, 99-U265.
4 N. Cox, M. Retegan, F. Neese, D. A. Pantazis, A. Boussac, W. Lubitz, *Science* 2014, ***345***, 804-808.
5 F. Jiao, H. Frei, *Energy Environ. Sci.* 2010, ***3***, 1018-1027.
6 G. C. Dismukes, R. Brimblecombe, G. A. N. Felton, R. S. Pryadun, J. E. Sheats, L. Spiccia, G. F. Swiegers, *Acc. Chem. Res.* 2009, ***42***, 1935-1943.
7 D. G. Nocera, *Acc. Chem. Res.* 2012, ***45***, 767-776.
8 P. Du, R. Eisenberg, *Energ Environ Sci* 2012, ***5***, 6012-6021.
9 V. Artero, M. Chavarot-Kerlidou, M. Fontecave, *Angew. Chem. Int. Ed.* 2011, ***50***, 7238-7266.
10 M. Dinca, Y. Surendranath, D. G. Nocera, *Proc. Natl. Acad. Sci. U.S.A.* 2010, ***107***, 10337-10341.
11 X. Yu, T. Hua, X. Liu, Z. Yan, P. Xu, P. Du, *ACS Appl. Mater. Interfaces* 2014, ***6***, 15395-15402.
12 W. C. Ellis, N. D. McDaniel, S. Bernhard, T. J. Collins, *J. Am. Chem. Soc.* 2010, ***132***, 10990-10991.
13 W. D. Chemelewski, H. C. Lee, J. F. Lin, A. J. Bard, C. B. Mullins, *J. Am. Chem. Soc.* 2014, ***136***, 2843-2850.
14 S. M. Barnett, K. I. Goldberg, J. M. Mayer, *Nat. Chem.* 2012, ***4***, 498-502.
15 Z. F. Chen, A. R. Rathmell, S. R. Ye, A. R. Wilson, B. J. Wiley, *Angew. Chem. Int. Ed.* 2013, ***52***, 13708-13711.
16 X. Liu, H. Jia, Z. Sun, H. Chen, P. Xu, P. Du, *Electrochem. Commun.* 2014, ***46***, 1-4.

17 A. R. J. Kucernak, V. N. N. Sundaram, *J. Mater. Chem. A.* 2014, ***2***, 17435-17445.
18 E. J. Popczun, J. R. McKone, C. G. Read, A. J. Biacchi, A. M. Wiltrout, N. S. Lewis, R. E. Schaak, *J. Am. Chem. Soc.* 2013, ***135***, 9267-9270.
19 A. Han, S. Jin, H. Chen, H. Ji, Z. Sun, P. Du, *J. Mater. Chem. A* 2015, ***3***, 1941-1946.
20 S. Cobo, J. Heidkamp, P. A. Jacques, J. Fize, V. Fourmond, L. Guetaz, B. Jousselme, V. Ivanova, H. Dau, S. Palacin, M. Fontecave, V. Artero, *Nat. Mater.* 2012, ***11***, 802-807.
21 N. Jiang, L. Bogoev, M. Popova, S. Gul, J. Yano, Y. J. Sun, *J. Mater. Chem. A.* 2014, ***2***, 19407-19414.
22 W. J. Zhou, X. J. Wu, X. H. Cao, X. Huang, C. L. Tan, J. Tian, H. Liu, J. Y. Wang, H. Zhang, *Energy Environ. Sci.* 2013, ***6***, 2921-2924.
23 Y. Z. Chen, H. D. She, X. H. Luo, G. H. Yue, D. L. Peng, *J. Cryst. Growth.* 2009, ***311***, 1229-1233.
24 J. Q. Tian, Q. Liu, A. M. Asiri, X. P. Sun, *J. Am. Chem. Soc.* 2014, ***136***, 7587-7590.
25 Z. H. Pu, Q. Liu, C. Tang, A. M. Asiri, X. P. Sun, *Nanoscale* 2014, ***6***, 11031-11034.
26 R. Franke, T. Chasse, P. Streubel, A. Meisel, *J Electron. Spectrosc.* 1991, ***56***, 381-388.
27 H. B. Lu, C. T. Campbell, D. J. Graham, B. D. Ratner, *Anal. Chem.* 2000, ***72***, 2886-2894.
28 Y. Y. Liang, Y. G. Li, H. L. Wang, J. G. Zhou, J. Wang, T. Regier, H. J. Dai, *Nat. Mater.* 2011, ***10.***, 780-786.
29 Y. Zhao, R. Nakamura, K. Kamiya, S. Nakanishi, K. Hashimoto, *Nat. Commun.* 2013, ***4***.
30 X. X. Yu, Z. J. Sun, Z. P. Yan, B. Xiang, X. Liu, P. W. Du, *J. Mater. Chem. A.* 2014, ***2***, 20823-20831.
31 X. J. Liu, Z. Chang, L. Luo, T. H. Xu, X. D. Lei, J. F. Liu, X. M. Sun, *Chem. Mater.* 2014, ***26***, 1889-1895.

